Preprint, version 1

Ru(II)–Pd(II) dinuclear complexes of di(pyridin-2-yl)amino-substituted 1,10-phenanthrolines: synthesis, characterization and application for catalysis †

Violetta A. Ionova, [a] Alena V. Dmitrieva, [a] Anton S. Abel, *[a] Aleksandr D. Sergeev, [a] Grigory S. Evko, [a] Alexei A. Yakushev, [a] Victoria E. Gontcharenko, [b,c] Sergei E. Nefedov, [d]‡ Vitaly A. Roznyatovsky, [a] Andrey V. Cheprakov, [a] Alexei D. Averin, [a] Tatiana V. Magdesieva, *[a] and Irina P. Beletskaya *[a,e]

[a] *Lomonosov Moscow State University, Department of Chemistry, 1-3, Leninskie Gory, Moscow, 119991, Russia; E-mail: antonabel@list.ru, tvm@org.chem.msu.ru.*

[b] *P.N. Lebedev Physical Institute of the, Russian Academy of Sciences, 53, Leninsky Prospect, Moscow, 119991 Russia;*

[c] *Higher School of Economics, Faculty of Chemistry, National Research University, 20 Miasnitskaya Street, Moscow, 101000 Russia;*

[d] *N.S. Kurnakov Institute of General and Inorganic Chemistry RAS, 119991, Leninsky pr., 31, Moscow, Russian Federation.*

[e] *Frumkin Institute of Physical Chemistry and Electrochemistry, Russian Academy of Sciences, Leninsky Pr. 31, Moscow, 119071, Russia; E-Mail: beletska@org.chem.msu.ru.*

‡ *Sergei E. Nefedov is deceased (November 6th, 2021).*

ABSTRACT

Dinuclear complexes bearing Ru(II) photoactive center are of interest for the development of efficient dual catalysts for many photocatalyzed reactions. Ditopic polypyrine ligands – bis(pyridine-2-yl)amino-1,10-phenanthrolines – containing additional coordination site (bis(pyridine-2-yl)amine, dpa) at positions 3, 4 or 5 of 1,10-phenanthroline core (**Phen-3NPy$_2$**, **Phen-4NPy$_2$** and **Phen-5NPy$_2$**) were synthesized. They were used as bridging ligands to obtain dinuclear complexes of composition [(bpy)$_2$Ru(**Phen-NPy$_2$**)PdCl$_2$](PF$_6$)$_2$ (**Ru(Phen-NPy$_2$)Pd**) via stepvise comlexing in good yields. Ru(II) is coordinated to 1,10-phenanthroline in these complexes, while Pd(II) is bound to dpa chelating moiety, which was established by NMR spectroscopy and X-ray single crystal analysis. The influence of the position of dpa in phenanthroline ring on the structural, optical and electrochemical properties of **Ru(Phen-NPy$_2$)Pd** complexes was studied. The complexes possess photoluminescence in argon-saturated MeCN solution with maxima in the range of 615–625 nm, emission quantum yields range from 0.11 to 0.15 for **Ru(Phen-NPy$_2$)** complexes and from 0.018 to 0.026 for dinucear **Ru(Phen-NPy$_2$)Pd** complexes. All the complexes have high extinction coefficients in the range of 370–470 nm, efficiently absorb visible light and can be used as photocatalysts. The Ru$^{2+/3+}$ potential in **Ru(Phen-NPy$_2$)Pd** complexes showed no significant dependence on dpa position, while

$Pd^{2+/0}$ reduction potential was quite lower for **Ru(Phen-3NPy$_2$)Pd** and **Ru(Phen-NPy$_2$)Pd**, than for **Ru(Phen-NPy$_2$)Pd** (–0.57V and –0.72V *vs* Ag/AgCl, $KCl_{(sat)}$, respectively). The behaviour of the complexes was studied in Cu-free Sonogashira coupling under blue LED (12 W) irradiation. The reaction proceeds three times faster when **Ru(Phen-4NPy$_2$)Pd** and **Ru(Phen-3NPy$_2$)Pd** are used as catalysts precursors than in the case of mixed catalytic system $Ru(bpy)_3(PF_6)_2$/$(RNPy_2)PdCl_2$.

INTRODUCTION

Dinuclear complexes combine a variety of useful properties due to the presence of two metallocenters in their structure, and owing to this feature they find applications in supramolecular assembles design, chemosensors, optoelectronic devices, smart materials, photoelectrodes components and photocatalysts[1-4]. Photoactive Ru(II) and Ir(III) complexes with various polypyridine ligands (2,2'-bipyridine, 1,10-phenanthroline, 2,2':6',2''-terpyridine, etc.) are frequently used as photoredox catalysts due to appropriate RedOx potentials, high extinction coefficients in the visible range of the spectrum, photostability and long lifetimes [5, 6]. One of their application is dual catalysis (or metallaphotoredox catalysis), combining photocatalysis under visible light irradiation and catalysis by metal complexes [7-11]. This metodology opens possibilities for the formation of carbon-carbon and carbon-heteroatom bonds under mild conditions thus enabling the synthesis of a wide range of valuable compounds [9]. The mechanism of dual photoredox-catalyzed processes implies the interaction between a photocatalyst (PC) and a metal complex *via* the electron or energy transfer (SET or EnT)[12]. Combining a sensitizer and a metal complex catalyst in one molecule often helps to optimize their interaction and to increase the activity of the catalytic system [13-16]. The advantages of the dinuclear photoactive complexes was thoroughly studied in such processes as hydrogen photogeneration[17-19], CO_2 photoreduction[14, 20, 21] and photoaccelerated polymerization[22-25]. In recent years Ir–Pd[26, 27], Ru–Pd[28, 29], Ru–Au[30], Ru–Cu [31, 32] and Ir–Ni [33] dinuclear complexes have been successfully employed for the oxydation reactions and carbon-carbon and carbon-element bond formation reactions under visible light irradiation. The structure of the bridging ligand is one of the most important parameters controlling the interaction between the photocatalyst and the metal complex catalyst in the dinuclear complex and thus governing the efficiency of the dual catalyst. Variation of the structure of the bridging ligand allows fine tuning the catalytic system in view of enhancing its activity[15, 34]. The nature of substituents in the heterocyclic ligand and their position in the core significantly influence spectral, electrochemical and catalytic properties of Ru complexes[35-39]. One may assume that binding metal complex and photocatalyst *via* various positions of the heterocyclic ligand (1,10-phenanthroline or 2,2'-bipyridine) will help to improve

photocatalyst properties. In spite of the sufficient number of works dealing with the bridging ligand optimization for better performance of supramolecular photocatalysts, variation of the poisition of the linker in the heterocyclic ligand has yet not been insufficiently studied [40, 41].

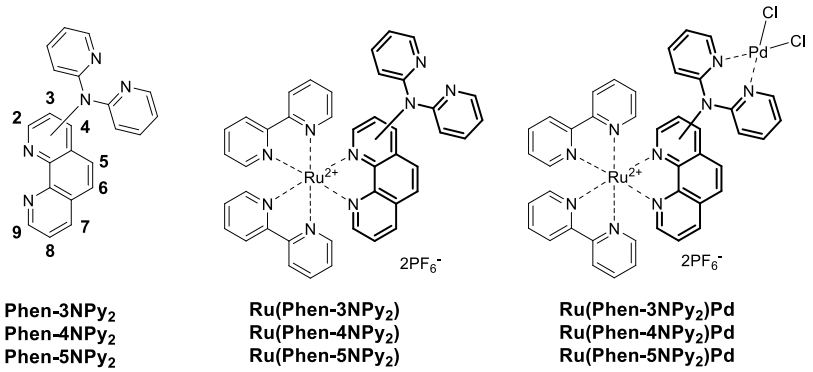

Fig. 1. Structures of investigated ditopic ligands and their Ru(II) complexes.

In this work, we have synthesized ditopic polypyridine ligands **Phen-NPy$_2$** based on 1,10-phenanthroline (phen) and di(pyridin-2-yl)amine (dpa) as an additional chelating unit at positions 3, 4, 5 of phenanthroline core (Fig. 1). These ligands were subjected to stepwise coordination to obtain **Ru(Phen-NPy$_2$)** and **Ru(Phen-NPy$_2$)Pd** complexes. Using NMR spectroscopy it was established that Ru(II) is coordinated by 1,10-phenanthroline and Pd(II) is coordinated by dipyridin-2-ylamine. The structures of three complexes were confirmed by X-ray analysis as well. Spectral, electrochemical investigations and DFT calculations demonstrate that the position of the dpa-substituent in the 1,10-phenanthroline core substantially influence the structure and properties of Ru–Pd dinuclear complex. Catalytic properties of **Ru(Phen-NPy$_2$)Pd** were studied using an exemplary visible-light-photoaccelerated copper-free Sonogashira reaction in which the complex with the dpa moiety at position 4 demonstrated the highest activity. The reaction rate was about 3 times higher than that of the mixed catalytic system $Ru(bpy)_3^{2+}$**/(NPy$_2$)Pd** under same conditions.

RESULTS AND DISCUSSIONS

Synthesis

The ligands were synthesized using copper-catalyzed amination from synthetically available bromo derivatives of 1,10-phenanthrolines and di(pyridin-2-yl)amine (Scheme 1). To note, in this reaction both reagents are good chelators which can bind copper and palladium thus hampering the catalytic reaction.

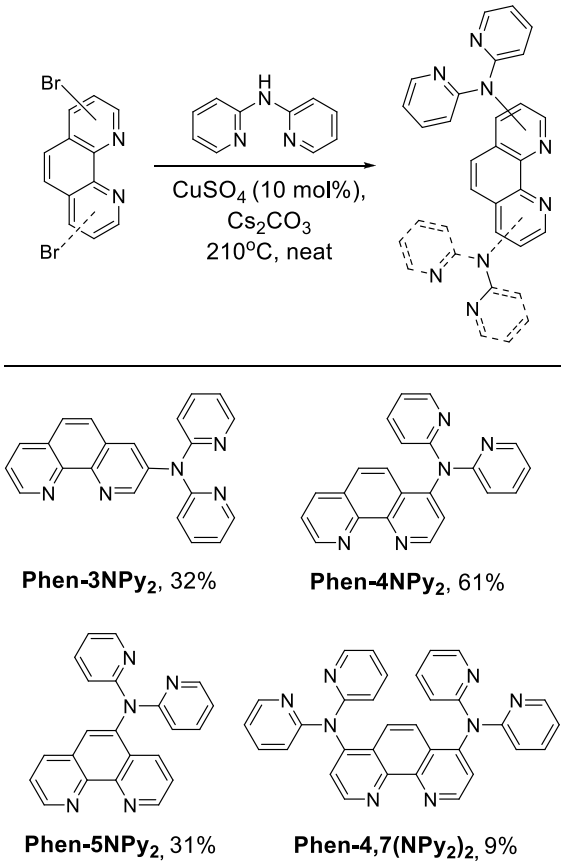

Scheme 1. Synthesis of ditopic ligands **Phen-NPy$_2$**.

Moderate yields were obtained under modified conditions which were proposed earlier for the arylation of bis(pyridin-2-yl)amine[42]. The reaction was conducted in the presence of copper(II) sulfate (10–20 mol%) and cesium carbonate (2 equiv.) taken as a base, at 210°C without solvent. **Phen-3NPy$_2$** and **Phen-5NPy$_2$** ligands were obtained in 32 and 31% yields, respectively. As bromine atom at *para*-position to the nitrogen atom in *N*-heterocycles is known to be more active in the catalytic substitution reaction, **Phen-4NPy$_2$** ligand was obtained in 61% yield. The reaction of 4,7-dibromo-1,10-phenanthroline with excess of di(pyridin-2-yl)amine in the presence of more catalyst and base led to a complex mixture, and the target **Phen-4,7(NPy$_2$)$_2$** was isolated in only 9%. Alternative synthetic routes including copper- and palladium-catalyzed amination, classical nucleophilic substitution were also studied (Tables S1, S2, Schemes S1, S2), but they were found to be inefficient.

Synthesis of **Ru(Phen-NPy$_2$)** complexes from *cis*-Ru(bpy)$_2$Cl$_2$ was carried out using microwave reactor according to a standard method previously described for the [Ru(**L**)(bpy)$_2$](PF$_6$)$_2$ complexes (Scheme 2). The complexes were isolated by sedimentation from the water-methanol solution by adding of NH_4PF_6 saturated water solution. If needed, additional purification can be achieved by the column chromatography. Preparative yields of the complexes ranged from 64 to 84%.

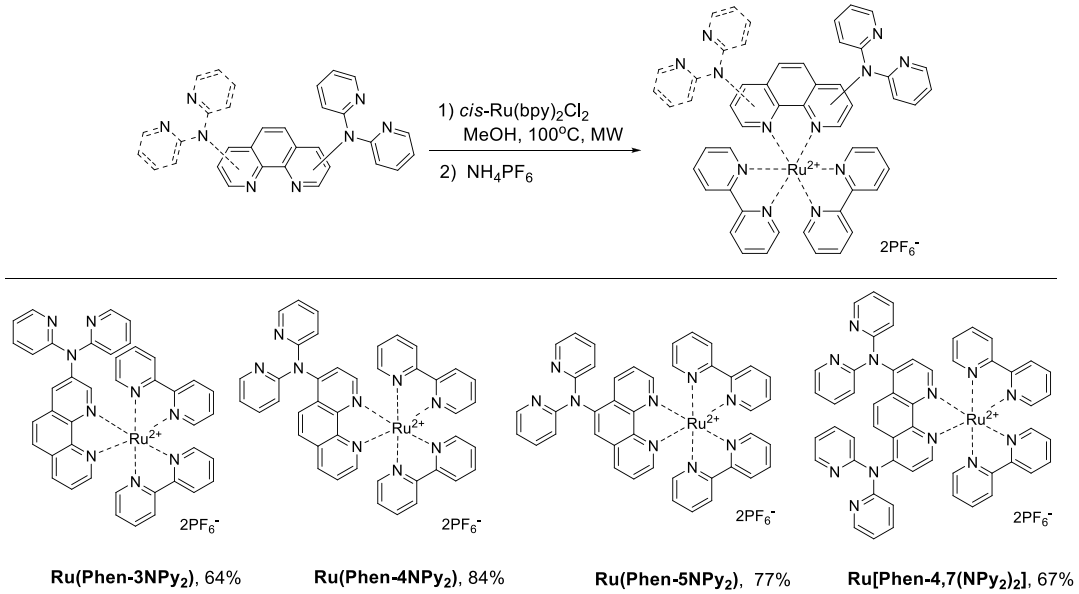

Scheme 2. Synthesis of Ru(II) complexes **Ru(Phen-NPy$_2$)**.

The nitrogen atoms in a rigid 1,10-phenanthroline moiety are preorganized for coordination unlike in di(pyridin-2-yl)amine in which nitrogen atoms are distant in a result of the steric repulsion of two pyridine rings. This ensures selective complexation and helps to avoid the formation of homodinuclear complexes without any special precautions like slow addition of the reagent, use of an excess of the ligand [19] or application of "chemistry on complex" approach [43] followed by a tedious separation of different complexes by size exclusion chromatography.

Ru(Phen-NPy$_2$)Pd heterodinuclear complexes were obtained *via* a standard method by reacting corresponding Ru complexes with $Pd(MeCN)_2Cl_2$ in dichloromethane at room temperature (Scheme 3). Target complexes were isolated in high yields (85–90%) as crystalline powders by slow addition of hexane to reaction mixtures.

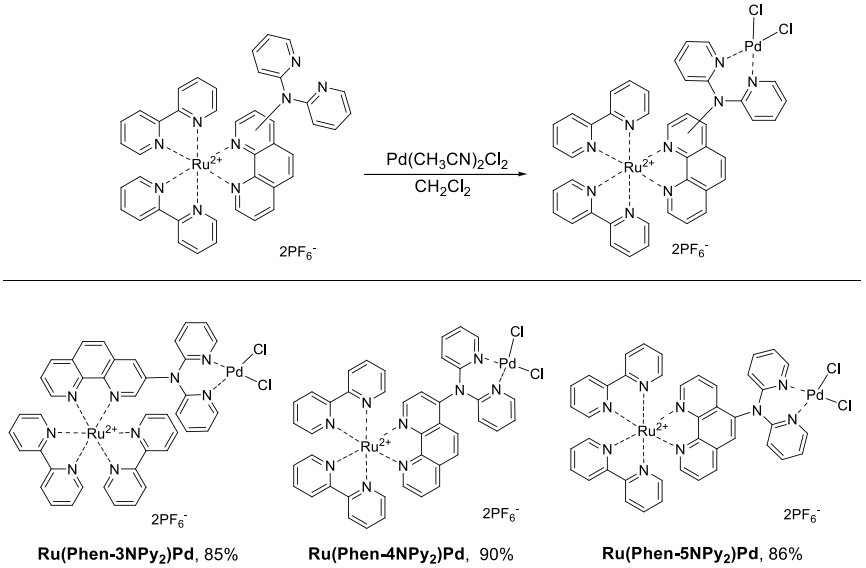

Scheme 3. Synthesis of dinuclear complexes **Ru(Phen-NPy$_2$)Pd**.

To study the effect of the combination of Pd and Ru complexes in one molecule, the same method was employed to obtain **(NPy$_2$)Pd** complex without the third heteroaromatic moiety at the nitrogen atom (Scheme 4). The corresponding ligand **NPy$_2$** was synthesized from 2-bromopyridine by the Buchwald-Hartwig amination reaction under classic conditions. The new ligands and complexes were characterized by NMR spectroscopy and mass spectrometry.

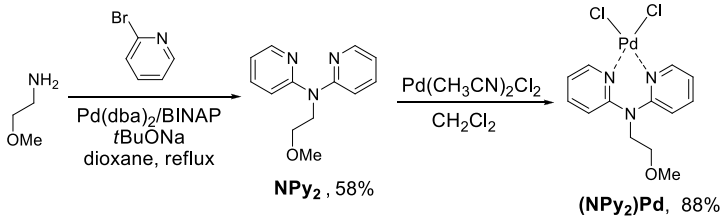

Scheme 4. Synthesis of **(NPy$_2$)Pd** complex.

Structural characterization in solution

The Ru and Ru–Pd complexes were studied by NMR spectroscopy in CD_3CN. Chemical shifts and coupling constants in ^{1}H and ^{13}C spectra are given in Tables S3–S8 in ESI. Signals in ^{1}H NMR spectra of free ligands can be easily attributed on the basis of coupling constants, integral intensities and additive schemes, while 2D NMR experiments are needed for characterization of the complexes. Attribution of the signals in the proton spectra to certain heterocycle (1,10-phenanthroline, 2,2'-bipyridine or 2-aminopyridine) was possible by COSY and TOCSY experiments, precise chemical shifts were obtained with PSYCHE method. In ^{13}C NMR spectra the attribution of tertiary carbon atoms was made by HSQCAD, and of quaternary carbon atoms – with HMBCAD technique. In the case of unsymmetric complexes it is difficult to attribute ^{1}H and ^{13}C signals of the pyridine rings to a certain 2,2'-bipyridine ligand [38]. In the case of **Ru(Phen-3NPy$_2$)**, **Ru(Phen-3NPy$_2$)Pd** and **Ru(Phen-4NPy$_2$)Pd** complexes proton signals at 3 and 3' positions of 2,2'-bipyridines are enough different due to the proximity of the substituent in the phen-ligand to Ru center, thus allowing full assignment using HMBCAD. In the case of **Ru(Phen-3NPy$_2$)** complex ROESY method can also be used to assign pyridine protons in 2,2'-bipyridine ligands using a cross-peak between the protons at 3 and 3' positions, the distance between them being 2.2 Å (Fig. S9). In other four complexes one may exclude only several combinations judging by the chemical shifts of the α-pyridine protons which are influenced by the ring currents of 1,10-phenanthroline or 2,2'-bipyridine.

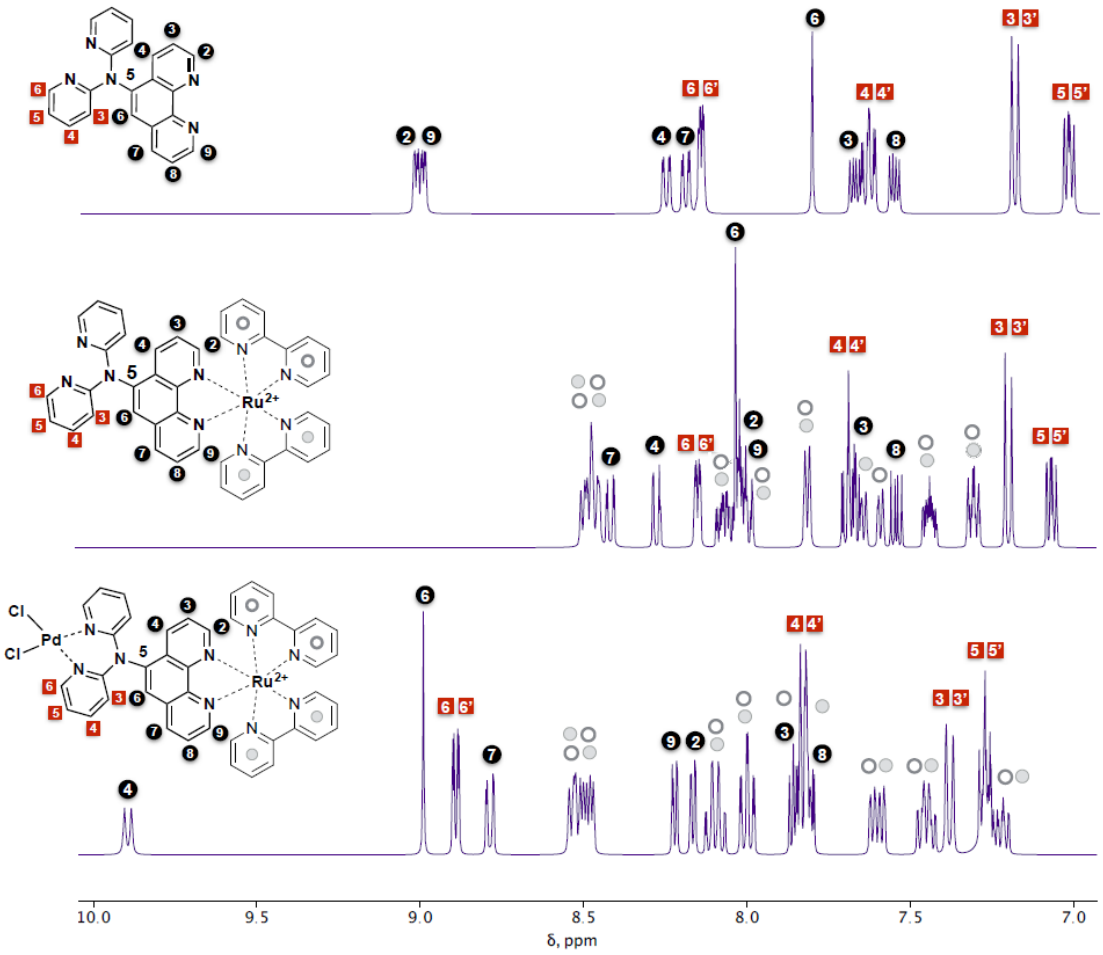

Fig. 2. ^{1}H-NMR spectra of **Phen-5NPy$_2$, Ru(Phen-5NPy$_2$)** and **Ru(Phen-5NPy$_2$)Pd** (top to bottom) in acetonitrile-*d3* at room temperature.

^{1}H NMR spectra for **Phen-5NPy$_2$** ligand and **Ru(Phen-5NPy$_2$)** and **Ru(Phen-5NPy$_2$)Pd** complexes in CD_3CN are given in Figure 2. Proton spectrum of **Ru(Phen-5NPy$_2$)** ligand is characterized by an upfield shift of H2 and H9 protons in 1,10-phenanthroline compared to the corresponding signal of the free ligand (form 9.09 to 8.06 ppm) due to the effect of the ring current of 2,2'-bipyridine which is a general feature of Ru polypyridine complexes [44, 45]. Protons of bis(pyridine-2-yl)amine moiety are characterized by almost the same chemical shifts as in a free ligand, which supports Ru coordination with 1,10-phenanthroline site. Moreover, the number of different signals in ^{1}H PSYCHE and ^{13}C{H} spectra manifest non-inequivalence of 2,2'-bipyridine ligands which correlated with the symmetry of the proposed structure of the complex (Fig. S16, S17). In the ^{1}H NMR spectrum of **Ru(Phen-5NPy$_2$)Pd** complex the signals of the dpa moiety are downfield shifted in comparison with **Ru(Phen-5NPy$_2$)** complex due to the coordination of Pd by this site. The most pronounced effect is noted for the 6-H protons of 2-aminopyridine group (shifted from 8.19 to 8.90 ppm) because of their proximity to Pd center. Analogous regularities were observed for **Ru(Phen-3NPy$_2$)**, **Ru(Phen-3NPy$_2$)Pd**, **Ru(Phen-**

4NPy$_2$) and **Ru(Phen-4NPy$_2$)Pd** complexes (Fig. S1 and S2), and it supports our conclusions on the coordination mode of two metals.

Also the signals of H4 and H6 protons of the 1,10-phenanthroline ligand in **Ru(Phen-5NPy$_2$)Pd** complex are substantially downfield shifted compared to **Ru(Phen-5NPy$_2$)** complex; in the case of the proton in a *peri*-position to bis(pyridine-2-yl)amine difference reaches 1.59 ppm (from 8.32 to 9.91 ppm). Such strong effect can be attributed not only to proximity of the palladium center to this proton but also to the anagostic interactions. In **Ru(Phen-4NPy$_2$)Pd** complex a similar downfield shift of the doublet corresponding to a proton in a *peri*-position is noted (Fig. S2), this can also indicate the anagnostic interaction of this hydrogen atom and palladium.

In the case of **Ru(Phen-3NPy$_2$)Pd** complex the signals of the protons in *ortho*-positions to dpa substituent (i.e. H2 and H4 of 1,10-phenanthroline) are upfield shifted (by *ca* 0.4 ppm in comparison with **Ru(Phen-3NPy$_2$)** complex) (Fig. S1). This can be caused by the conjugation of nitrogen lone pair of the nitrogen with phenathroline π-system. Thus, the geometry of Ru–Pd complexes allows anagostic Pd-H interactions only for *peri*-protons.

To sum up, NMR experiments confirm that **Phen-NPy$_2$** ligands form Ru(II) complexes through 1,10-phenanthroline site and Pd(II) complexes are formed *via* dpa site. Also, **Ru(Phen-5NPy$_2$)Pd** and **Ru(Phen-4NPy$_2$)Pd** complexes are characterized by anagostic interactions between Pd and the protons in *peri*-positions to dpa fragment (H4 and H5, respectively).

Structural characterization in solid-state

We managed to obtain crystals suitable for structural analysis for the mononuclear complexes **Ru(Phen-5NPy$_2$)** and **(NPy$_2$)Pd** and dinuclear complexes **Ru(Phen-3NPy$_2$)Pd** and **Ru(Phen-4NPy$_2$)Pd** by slow diffusion of toluene into the solution of the complex in CH_2Cl_2 or $CHCl_3$/MeOH mixture. The crystal parameters and data collection details are given in Tables 1 and S9, ORTEP diagrams are shown in Fig. 3, additional information on refinement method, treatment of solvent molecules and disordered groups are given in ESI.

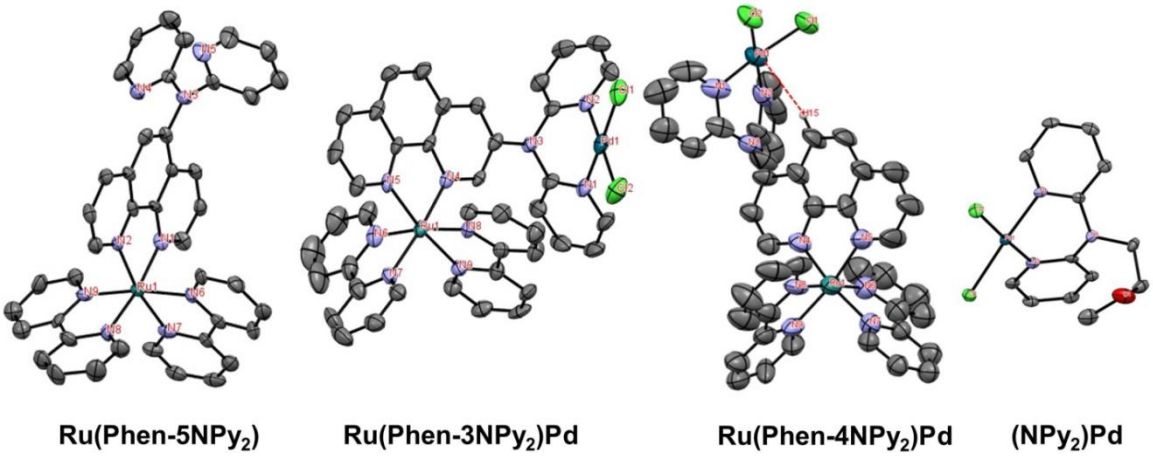

Fig. 3. X-Ray structures of **Ru(Phen-5NPy$_2$)**, **Ru(Phen-3NPy$_2$)Pd**, **Ru(Phen-4NPy$_2$)Pd** and **(NPy$_2$)Pd**. Ellipsoids are at the 50% probability level. H atoms, PF_6 counter anions, co-crystallized solvent molecules and disorders are omitted for clarity. Anagostic interaction supposed in **Ru(Phen-4NPy$_2$)Pd** is shown by red dotted line.

Ru-containing complexes crystallize in the triclinic system with P-1 space group while **(NPy$_2$)Pd** is most stable in the orthorhombic crystal system with Pbca symmetry. Ruthenium atom in **Ru(Phen-5NPy$_2$)**, **Ru(Phen-3NPy$_2$)Pd** and **Ru(Phen-4NPy$_2$)Pd** complexes is coordinated to 1,10-phenanthroline site of the ditopic ligand. In all cases the ruthenium atom has a slightly distorted octahedral environment formed by six nitrogen atoms of 1,10-phenanthroline and two 2,2'-bipyridines (Ru–N 2.06–2.09 Å, N–Ru–N 78.6–80.4 °) similar to previously reported ruthenium polypirydine complexes [37, 46, 47]. Despite the significant volume of the substituent, its position in the phenanthroline core does not have a significant effect on these parameters. Palladium atom in **Ru(Phen-3NPy$_2$)Pd**, **Ru(Phen-4NPy$_2$)Pd** and **(NPy$_2$)Pd** complexes is similarly coordinated to bis(pyridin-2-yl)amine site through two heterocyclic nitrogen atoms. Two chlorine ions in *cis*-position complete square N_2Cl_2 coordination environment. Ligand and palladium atom form a six-membered chelate ring with a boat conformation. Two pyridine rings form dihedral angles 50.12(15)^o, 60.8(3)^o and 44.3(4)^o in **NPy$_2$Pd**, **Ru(Phen-3NPy$_2$)Pd** and **Ru(Phen-4NPy$_2$)Pd**, respectively. Pd–N and Pd–Cl distances and N–Pd–N and Cl–Pd–Cl angles are in a typical range for a (dpa)$PdCl_2$-type core[48, 49]. In the case of **(NPy$_2$)Pd** the oxygen atom is not coordinated to palladium atom either in intermolecular or intramolecular manner.

Table 1. Selected crystallographic data, bond distances (Å) and angles (deg) for **Ru(Phen-5NPy$_2$), Ru(Phen-3NPy$_2$)Pd, Ru(Phen-4NPy$_2$)Pd** and **(NPy$_2$)Pd**.

Parameter	Ru(Phen-5NPy$_2$)	Ru(Phen-3NPy$_2$)Pd	Ru(Phen-4NPy$_2$)Pd	(NPy$_2$)Pd
Cryst. syst.	triclinic	triclinic	triclinic	orthorhombic
Space group	$P\bar{1}$	$P\bar{1}$	$P\bar{1}$	Pbca
a/Å	10.1007(8)	12.804(1)	12.689(8)	12.032(1)
b/Å	13.393(1)	12.979(1)	14.266(9)	15.188(1)
c/Å	17.789(2)	17.639(1)	14.621(9)	16.297(1)
α/deg	70.753(5)	86.755(3)	84.68(1)	90
β/deg	76.873(4)	71.875(2)	88.88(1)	90
γ/deg	69.270(4)	76.129(3)	83.02(1)	90
Ru–N^{L}/ Å	2.06–2.09(1)	2.043(5)–2.071(5)	2.038(8)–2.083(8)	–
N^{Phen}–Ru–N^{Phen} / deg	79.1(4)	79.7(2)	80.4(3)	–
N^{bpy}–Ru–N^{bpy} / deg	78.6(4), 78.0(4)	79.4(2), 79.1(2)	77.7(4), 79.1(3)	–
Pd–N^{Py}/ Å	–	2.019(7), 2.028(6)	1.919(8), 2.161(9)	2.015(3), 2.020(3)
Pd–Cl/ Å	–	2.279(2), 2.270(3)	2.264(4), 2.283(5)	2.284(1), 2.298(1)
N^{py}–Pd–N^{py} / deg	–	87.4(2)	87.0(3)	86.4(1)
Cl–Pd–Cl / deg	–	91.1	90.1	90.9

In **Ru(Phen-5NPy$_2$)** complex pyridine rings of dpa substituent have a propeller-type orientation to minimize steric hindrance the lone electron pair of the central nitrogen atom is conjugated with π-system of one of the pyridine rings. **Ru(Phen-3NPy$_2$)Pd** and **Ru(Phen-4NPy$_2$)Pd** complexes show quite different orientation of dpa moiety. Thus, in **Ru(Phen-3NPy$_2$)Pd** complex (dpa)$PdCl_2$ unit is oriented sideways to minimize steric hindrance with the protons at *ortho*-positions (H2 and H4) of the 1,10-phenanthroline ring. As a result, the palladium atom is located at its maximum distance from the 1,10-phenanthroline plane (dihedral angle 92 °) and lone electron pair of the central nitrogen atom is conjugated with π-system of 1,10-phenanthroline which is consistent with the data obtained by NMR.

In the case of **Ru(Phen-4NPy$_2$)Pd** complex, the palladium atom is disordered over two positions, both of them practically being in the plane of the phenanthroline ring. Such orientation can be explained by the presence of strong anagostic interactions between the palladium and the hydrogen atom in the *peri*-position 5 of the 1,10-phenanthroline core. Pd…H distance (Fig. 2, red dotted line) and C–H…Pd angle are 2.992(2) Å and 164.8(6) °, respectively, which correspond to geometric parameters for such type of interaction [50]. Needless to say, this assumption should have been taken with grain of salt due to the overall low quality of X-ray diffraction data associated with the presence of disorder, which resulted not only in two crystallographic positions of palladium atom, but also in high uncertainty in Pd…H distance caused by the treatment of hydrogen atoms in the refinement process. Nevertheless, the claim

about the presence of anagostic interactions was supported by the downfield shift of the signal of this proton relative to **Ru(Phen-4NPy$_2$)** observed in the ^{1}H NMR spectrum (from 7.94 to 9.43 ppm, Fig. S1). Basing on NMR spectra and structural analysis we conclude the presence of anagostic interactions between palladium and the hydrogen atom in the *peri*-position in complexes **Ru(Phen-5NPy$_2$)Pd** and **Ru(Phen-4NPy$_2$)Pd**, which tends to be actual both in solution and in the solid state. Thus, the position of (dpa)PdCl$_2$-complex link to phenanthroline ring significantly influences their geometry and orientation. The results also support the proposed coordination mode of the ruthenium and palladium by **Phen-NPy$_2$** ligands after two-step complexation.

Electrochemistry

Catalytic cycles of Pd-catalyzed reactions and formation of catalyst from precatalyst commonly include several redox events with the Pd-based intermediates involved. Therefore, electrochemical study of the dinuclear **Ru(Phen-3NPy$_2$)Pd**, **Ru(Phen-4NPy$_2$)Pd** and **Ru(Phen-5NPy$_2$)Pd** complexes differing in the position of the dpa moiety (3-, 4- or 5-) in the 1,10-phenanthroline core as well as the model **(NPy$_2$)Pd** complex was performed, for comparative assessment of the propensity of the complexes to undergo redox transitions. Electrochemical measurements were performed at a Pt disk electrode in acetonitrile solution containing Bu$_4$NBF$_4$ as a supporting electrolyte. The voltammetry data obtained are given in Table 2 and Table S10, the voltammetry curve observed for complex **Ru(Phen-5NPy$_2$)Pd** taken as an example is given in Fig. 4; the voltammetric curves for the other complexes as well as the semi-differential and semi-integral curves are given in Fig. S40–50.

Table 2. Half-wave and peak potentials (V, *vs* Ag/AgCl, KCl$_{(sat)}$) of the **Ru(L)Pd** complexes and reference compounds in MeCN containing 0.05 M TBAPF$_6$ (Pt electrode).

Complex	$E^{Ox}_p(E^{Ox}_{1/2})$, V	$-E^{Red}_p(-E^{Red}_{1/2})$, V			
	$Ru^{2+/3+}$	$Pd^{2+/0}$	$L^{0/\bullet-}$	$L^{\bullet-/-2}$	$L^{2-/3-}$
Ru(bpy)$_3$ [a]	(1.36)	-	(1.25)	(1.44)	(1.68)
Ru(Phen)$_3$ [a]	(1.37)	-	1.68 (1.29)	1.81 (1.41)	-
Ru(Phen) [a]	(1.37)	-	(1.25)	(1.43)	(1.70)
(NPy$_2$)Pd	-	0.88	-	-	-
Ru(Phen-3NPy$_2$)Pd	1.42 (1.39)	0.57	1.28 (1.25)	1.46 (1.43)	1.74
Ru(Phen-4NPy$_2$)Pd	1.42 (1.38)	0.57	1.28 (1.24)	1.45 (1.38)	1.72
Ru(Phen-5NPy$_2$)Pd	1.43 (1.40)	0.72	1.25 (1.22)	1.45 (1.39)	1.73

[a] Values derived from data from ref. [37]

All studied Ru–Pd dinuclear complexes exhibited Ru-centered reversible diffusion-controlled (see ESI) one-electron oxidation, with almost identical $E_{1/2}$ potential values, corresponding to the $Ru^{2+/3+}$ redox couple (for comparison, the previously reported oxidation potential value for $[(bpy)_2Ru(Phen)]^{2+}$ (**Ru(Phen)**) is 0.975 V vs Ag^+/Ag [37] that corresponds to 1.37 V vs Ag/AgCl, $KCl_{(sat.)}$ in our conditions).

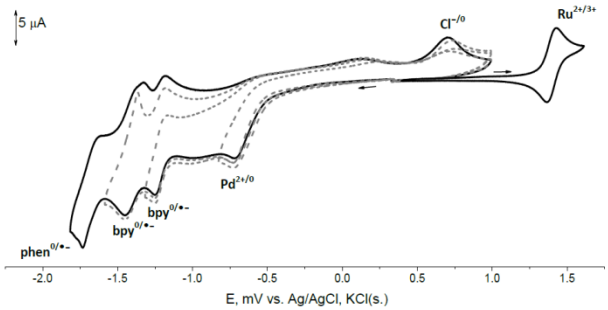

Fig. 4. Voltammetry curves observed for **Ru(Phen-5NPy$_2$)Pd** complex (Pt, CH_3CN, 0.05 M Bu_4NBF_4, vs. Ag/AgCl/KCl, 100 mV/s)**.**

The voltammetric behavior in the cathodic region was richer, four consecutive redox transformations were observed. The first cathodic peak was irreversible, two-electron (see ESI) and Pd-centered, as follows from the comparison to the reduction potential value determined for the model **(NPy$_2$)Pd** complex (E_p = 0.88 V vs Ag/AgCl, $KCl_{(sat.)}$). In the reverse scan, the characteristic peak corresponding to the oxidation of chloride ions can be observed (Fig. 4). The anodic shift in the first cathodic peak observed for the Ru–Pd bimetallic complexes vs. the reference **(NPy$_2$)Pd** complex is attributed to the electron-withdrawing effect of the ruthenium moiety. Notably, the $Pd^{2+/0}$ peak potential values for **Ru(Phen-3NPy$_2$)Pd** and **Ru(Phen-4NPy$_2$)Pd** complexes were identical. Though the conjugation of the 3-$N(Py)_2$ ligand with the N atom coordinated to the Ru center is disrupt (in contrast to its counterpart linked at position 4), the distortion of the co-planarity of the two fragments smoothers out the possible influence of the conjugation.

In contrast to **Ru(Phen-3NPy$_2$)Pd** and **Ru(Phen-4NPy$_2$)Pd** complexes in which the Pd-containing fragments are attached to the N-containing phenantroline ring, the Pd-centered reduction of **Ru(Phen-5NPy$_2$)Pd** complex was significantly shifted cathodically (for 150 mV). The probable reason is the following. The Pd-containing fragment is linked to the double bond of the phenantroline central ring which is less influenced by the electron-withdrawing effect of the N atoms coordinated to the Ru center.

The consecutive bipyridyl- and phenanthroline-centered reductions occur at similar potential values for all three complexes and are in a good agreement with the literature data (the

$E_{1/2}$ values determined for **Ru(Phen)** were as follows: –1.645, –1.83, –2.09 V vs Ag^+/Ag that correspond to –1.25, –1.44, –1.70 V vs Ag/AgCl, $KCl_{(sat.)}$ under our conditions [37]).

Thus, the position of the dpa moiety in the phenathroline core in the **Ru(Phen-NPy$_2$)Pd** complexes does not have any significant influence on $Ru^{2+/3+}$ potential value, but dramatically effects $Pd^{2+/0}$ reduction potential in **Ru(Phen-5NPy$_2$)Pd**. Based on the voltammetry data, one can assume that **Ru(Phen-5NPy$_2$)Pd** complex would be less active in catalysis if Pd^{2+} to Pd^0 reduction were the rate limiting step.

Absorption and emission properties

Absorption and emission properties of the **Ru(Phen-NPy$_2$)** и **Ru(Phen-NPy$_2$)Pd** complexes were studied in acetonitrile. UV-vis и emission spectra are given in Fig. S51, the main results for the complexes and reference compounds are given in Table 3. The most characteristic examples are presented in Fig. 5a,b. The absorption spectra of the complexes demonstrate a broad band in 380–500 nm region with a maximum *ca* 450 nm which corresponds to Ru-centered MLCT transitions and interligand LLCT transitions. Also, two intensive bands in 260–290 nm region are observed which can be attributed to ligand-centered (LC) π–π* transitions [51]. In the case of **Ru(Phen-3NPy$_2$)** and **Ru(Phen-3NPy$_2$)Pd** complexes one may observe also a band in 340–370 nm region (Figure 5a). It is characteristic for Ru complexes of 3-aminosubstituted 1,10-phenanthrolines [36, 52, 53] and probably corresponds to an interligand bpy/phen-based LLCT transition [54]. To note, coordination of palladium with dpa moiety in **Ru(Phen-3NPy$_2$)** leads to a hypsochromic shift of this band from 369 to 343 nm. Analogous shift was observed by us earlier upon the formation of the dinuclear Ru–Cu complex of 3-aminosubstituted phenanthroline possessing a chelating block [53]. In our case this shift seems to be unexpected because amino group do not participate in complexation.

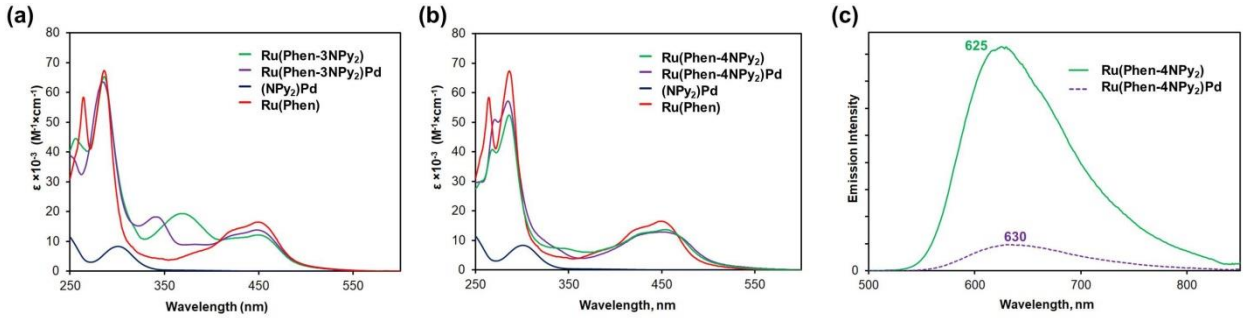

Fig. 5. Comparison of the absorption spectra of **(a) Ru(Phen-3NPy$_2$)** and **Ru(Phen-3NPy$_2$)Pd** and **(b) Ru(Phen-4NPy$_2$)** and **Ru(Phen-4NPy$_2$)Pd** with reference compounds (**Ru(Phen)** and **(NPy$_2$)Pd**) in acetonitrile. **(c)** Luminescence spectra of **Ru(Phen-4NPy$_2$)** and **Ru(Phen-4NPy$_2$)Pd** in Ar-saturated acetonitrile (λ_{ex} = 450 nm, C = 6 μM).

Introducing of dpa moiety to a 1,10-phenanthroline ligand practically does not influence the absorption bands corresponding to MLCT transition, both in Ru and in Ru-Pd complexes (Figures 5a,b). Extinction coefficients in these complexes only slightly differ from those in model compounds **Ru(bpy)$_3$** и **Ru(Phen)** (Table 3). It means that the obtained complexes can absorb visible light as efficiently as standard photocatalysts. Moreover, this ability of dinuclear **Ru(Phen-NPy$_2$)Pd** complexes strongly distinguish them from **(NPy$_2$)Pd** which is characterized by a single absorption band in UV region (301 nm, Figures 5a,b).

Photoluminescence spectra of **Ru(Phen-NPy$_2$)** and **Ru(Phen-NPy$_2$)Pd** complexes were registered in Ar-saturated acetonitrile (Table 3). Quantum yields of **Ru(Phen-NPy$_2$)** complexes are higher than that of **Ru(Phen)** complex without dpa substituent, and the highest quantum yield (0.15) was obtained for **Ru(Phen-4NPy$_2$)** complex. Emission maxima are slightly red shifted, more pronounced effect was registered for the complexes with dpa at positions 4 (20 nm) and 4,7 (25 nm). This effect is opposite to one observed by us previously for phenanthroline-containing $[(\mathbf{L})Ru(bpy)_2]^{2+}$ complexes with alkylamino substituents, in which quantum yields decreased, especially in the case of 4-amino-1,10-phenanthroline ligand [36]. One may assume that the presence of two electron withdrawing pyridine groups at the nitrogen atom neutralize the influence of its electron pair on the π-system of 1,10-phenanthroline in the complex. The absence of NH bond in the complex diminishes vibrational relaxation as compared to previously described complexes.

Table 3. Selected photophysical parameters of **Ru(bpy)$_3$**, **Ru(L)** and **Ru(L)Pd** complexes [a]

Complex	λ_{abs} [nm] (ε [× 10^3 × M^{-1} × cm^{-1}])	λ_{em}, [nm]	Φ (Ar) [b]
Ru(bpy)$_3$ [c]	286 (85.0), 451 (14.0)	609	0.095
Ru(Phen) [c]	272 (42), 283 (49), 450 (12)	605	0.096(6)
Ru(Phen-3NPy$_2$)	256 (41), 286 (63), 369 (19), 449 (12)	616	0.10(3)
Ru(Phen-4NPy$_2$)	268 (40), 286 (52), 454 (13.8)	625	0.15(3)
Ru(Phen-5NPy$_2$)	265 (32), 285 (42), 450 (9.1)	616	0.11(2)
Ru[Phen-4,7(NPy$_2$)$_2$]	256 (37), 287 (65), 349 (12), 452 (17.8)	630	0.11(3)
Ru(Phen-3NPy$_2$)Pd	285 (62), 343 (17.6), 382 (9.2), 448 (13.4)	615	0.020(6)
Ru(Phen-4NPy$_2$)Pd	270 (52), 285 (59), 450 (13.5)	630	0.018(4)
Ru(Phen-5NPy$_2$)Pd	265 (36), 286 (44), 450 (10.4)	624	0.026(7)

[a] Measurements were conducted in an argon-saturated acetonitrile at 298 K, λ_{em} = 450 nm; [b] Measured in an Ar-saturated solvent relative to a solution of Ru(bpy)$_3$ in acetonitrile as a standard [55]; [c] Data taken from [37] .

Palladium coordination to dpa block leads to a decrease in the quantum yields of the complexes emissions down to 1.8–2.6% which is usually explained by a more intensive intramolecular electron transfer process from Ru(II) to Pd atom [23], the most pronounced effect was observed with **Ru(Phen-4NPy$_2$)Pd** complex in which dpa moiety is in *para*-postion to the nitrogen atom of 1,10-phenenathroline. Luminescence intensity diminishes seriously (Fig. 5c), and the emission maximum shifts from 625 to 630 nm. The emission maximum does not change in **Ru(Phen-3NPy$_2$)Pd** complex in comparison with a palladium-free analogue **Ru(Phen-3NPy$_2$)**, but the largest difference is observed for **Ru(Phen-5NPy$_2$)** and **Ru(Phen-5NPy$_2$)Pd** complexes (616 and 624 nm, respectively). It is thought that the red shift of the luminescence maximum in such systems is a result of lowering energy level of π* of the phenanthroline ligand and reduction of energy gap [56].

Thus, the complexes obtained are able of absorbing visible light as efficiently as standard Ru complexes and can be regarded as photocatalysts.

DFT studies

DFT computations were performed on three bimetallic photocatalysts. The full geometry optimization was performed using the Firefly quantum chemistry package[57], which is partially based on the GAMESS (US) [58] source code. with B3LYP functional and JorgeDZ all electron basis set for all elements including Ru and Pd[59]. The optimized geometries, atom coordinates, frontier orbitals' isodensity plots and energies are given in ESI. Selected bond lengths and angles are summarized in Table S11, which are in good agreement with X-ray diffraction data wherever available. We and others earlier found that this level of computations is particularly well suited for geometry optimization of molecules involving either heavier main group elements and transition metals of the 1st and 2nd rows, being an optimal choice both from the viewpoint of accuracy and computation time, even though it avoids the approximation of core shells by a pseudopotential.[37] Morevover, it is the only basis set among those routinely used, which gives a trustworthy description of some fine features in the structure. Thus, in this work the X-ray structure of one of the complexes unexpectedly revealed the anagostic interaction between one of the protons and Pd atom, confirmed also in NMR spectra in solution. This interaction was confirmed by DFT computation of **Ru(Phen-4NPy$_2$)Pd** (Fig. 6a) only when JorgeDZ basis set was employed for all atoms to reveal that the conformation involving this interaction is the most stable on scanning the rotation of Pd-containing residue around the bond attaching it to the phenanthroline ligand of the Ru complex.

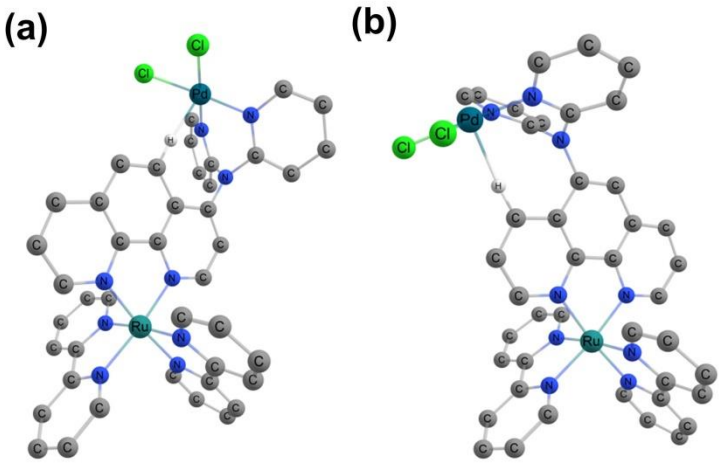

Fig. 6. The optimized geometry of **Ru(Phen-4NPy$_2$)Pd** (left) and **Ru(Phen-5NPy$_2$)Pd** (right) complexes (B3LYP/JorgeDZ for all atoms). Hydrogen atoms are ommited for clarity.

A similar anagostic interaction was identified by computations of **Ru(Phen-5NPy$_2$)Pd** (Fig. 6b) for which we failed to obtain a reasonable quality X-ray diffraction data. The calculated energy diagram of the frontier orbitals and HOMO and LUMO isodensity plots is presented in Fig. 7. Energies and isodensty plots of the frontier orbitals are given in more detail in Tables S12–S18. In all the complexes modeled LUMO$_{0+3}$ are localized on the ligand π* orbitals of Ru complex, mostly those of bpy peripheral ligands, in a few cases involving also phen ligand. The HOMOs are on the other hand built differently constructed quite different for each complex. In **Ru(Phen)** complex the uppermost HOMO is formed by Ru d-orbital, while in the case of **Ru(Phen-3NPy$_2$)** HOMO is built mostly by π-orbitals of 2-aminopyridine residue involving a contributions of d-orbital Ru atom and π-orbitals of phen. In **Ru(Phen-5NPy$_2$)** only the 2-aminopyridine orbitals are involved in the HOMO. The HOMO of **Ru(Phen-4NPy$_2$)** on the contrary is formed by d-orbitals of Ru atom and π-orbitals of phenanthroline ring and lone electron pair of aminogroup. HOMO orbitals of dinuclear Ru–Pd complexes are localized mainly on Pd and Cl atoms.

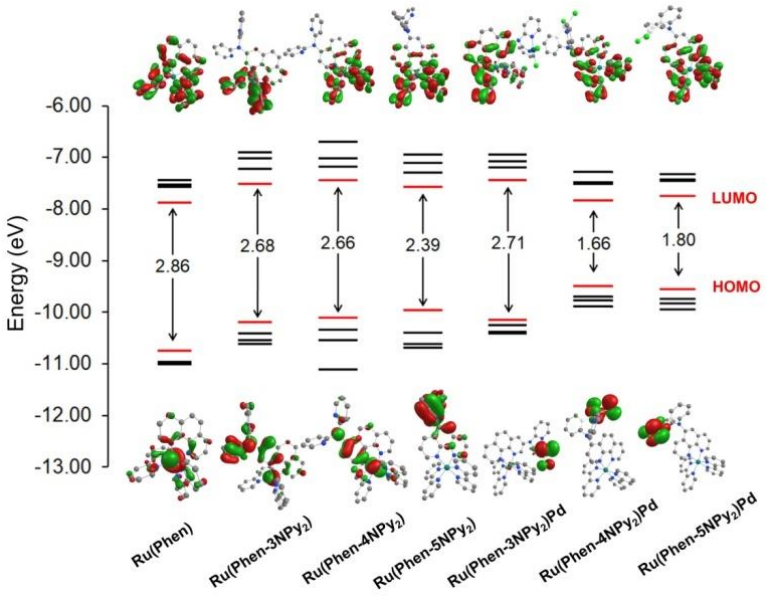

Fig. 7. Frontier orbital energies obtained from DFT calculations and HOMO and LUMO orbitals isodensity plots for **Ru(Phen)**, **Ru(Phen-NPy$_2$)** and **Ru(Phen-NPy$_2$)Pd** complexes.

It should be noted that correct modeling of ground and exited states of Ru polypyridine complexes requires sophisticated methods and still inconsistences of experimental and calculated data may take place [37, 60] so only qualitive analysis was performed in frames of this work. The 400–500 nm band in the UV-vis corresponding to MLCT is quite broad to analyze because of consisting of multiple metal-ligand transitions. HOMO–LUMO gaps of **Ru(Phen-NPy$_2$)** complexes were calculated to be smaller than in the case of **Ru(Phen)**. In the case of Ru–Pd dinuclear complexes calculated HOMO–LUMO gap is quite different. In the case of **Ru(Phen-3NPy$_2$)** and **Ru(Phen-3NPy$_2$)Pd** the decrease of the energy gap is almost absent, while **Ru(Phen-4NPy$_2$)Pd** and **Ru(Phen-5NPy$_2$)Pd** have much smaller gap than corresponding **Ru(L)** complexes, the minimum energy gap belongs to **Ru(Phen-4NPy$_2$)Pd**.

Photocatalytic properties

Catalytic properties of the dinuclear complexes were studied using a visible-light-photoaccelerated Cu-free Sonogashira reaction as a typical cross-coupling reaction normally catalyzed by Pd(0) species commonly accompanied by Cu(I) co-catalysts. This process was conducted in the presence of Ru(bpy)$_3$ on powerful irradiation (150 W) by Akita and coauthors [61] and is useful for the comparison of the efficiency of photoactive Pd-containing complexes [27, 62] despite the nature of this phenomenon has not yet been established.

The coupling of 4-iodoanisole with phenylacetylene was chosen as a model reaction (Fig. 8). The catalytic activity was tested for **Ru(Phen-3NPy$_2$)Pd**, **Ru(Phen-4NPy$_2$)Pd** and **Ru(Phen-**

5NPy$_2$)Pd dinuclear complexes, which bear dpa residue attached to 3, 4 or 5-position of phenanthroline, and the mixed catalytic system **Ru(bpy)$_3$/(NPy$_2$)Pd**. The conditions were initially optimized to achieve the highest yield of the cross-coupling product provide the best selectivity of the reaction and suppress diine formation (Table S19). The reactions were carried out in the presence of phosphine ligands to intercept Pd(0) species and exclude catalyst deactivation. Triphenylphosphine (Pd:L = 1:2) was ultimately chosen as an optimal choice, which is not surprising as the more specialized ligands are not required for reactions of aryl iodides. The loading of photocatalysts was kept at 1 mol%. Reactions were carried out in degassed DMF under argon and blue light irradiation (blue LEDs , 455 nm, 12 W, Fig. S53). Triethylamine was used as a base.

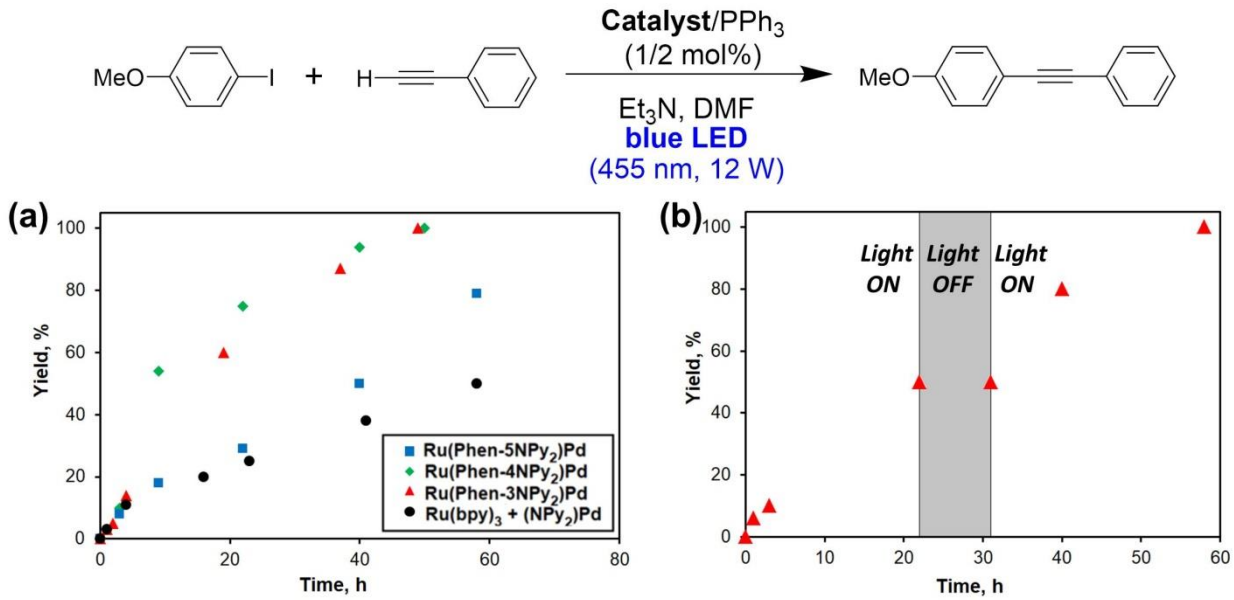

Fig. 8. NMR-monitoring of the Sonogashira coupling reaction catalyzed by dinuclear complexes (**Ru(Phen-3NPy$_2$)Pd**, **Ru(Phen-4NPy$_2$)Pd**, **Ru(Phen-5NPy$_2$)Pd** and mixed catalytic system (**Ru(bpy)$_3$/(NPy)$_2$Pd**). Reaction conditions: phenylacetylene (0.25 mmol), 4-iodoanisole (0.2 mmol), photocatalyst (1 mol%), Ph$_3$P (2 mol%), Et$_3$N (1 mL), DMF (4 mL), argon atmosphere, Schlenk tube, blue LED (12 W), r.t. The yields were determined by NMR ^{1}H analysis of samples taken from reaction mixtures. (a) Yields of 1-methoxy-4-(phenylethynyl)benzene in samples of reaction mixtures taken at varying time intervals; (b) Catalytic activity of **Ru(Phen-3NPy$_2$)Pd** under ON/OFF irradiation.

The pre-activation period is practically impossible to observe due to the low conversion values. During the first 3 hours, the product is formed at approximately the same rate in the case of both binuclear complexes and the **Ru(bpy)$_3$/Pd(NPy$_2$)** mixture (Figure 8a). However, over the next 60 hours there is a significant difference in the product formation rates. In the case of a mixed catalytic system, the reaction slows down significantly; in the case of the **Ru(Phen-**

5NPy$_2$)Pd precatalyst the product is formed only at a slightly higher rate. In the case of the **Ru(Phen-3NPy$_2$)Pd** and **Ru(Phen-4NPy$_2$)Pd** complexes, the reaction rate remains almost the same as at the initial stage.

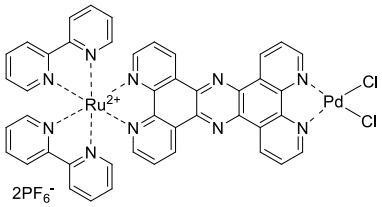

Ru(tpphz)Pd

Fig. 9. Ru(tpphz)Pd complex.

We also studied **Ru(tpphz)Pd** dinuclear complex (Fig. 9) based on well known bridging ligand under the same conditions, but the rate of the reaction appeared to be lower than in the case of **Ru(Phen-3NPy$_2$)Pd** and **Ru(Phen-4NPy$_2$)Pd** (Table S19, entries 19, 20). Thus, only 60% yield was achieved after 48 h of irradiation.

Ru(Phen-4NPy$_2$)Pd dinuclear complex under optimized conditions allows the synthesis of diarylacetylenes in good yields using reagents with both electron donor and electron withdrawing substituents (Table 4).

Table 4. Photoaccelerated arylation of arylacetylenes

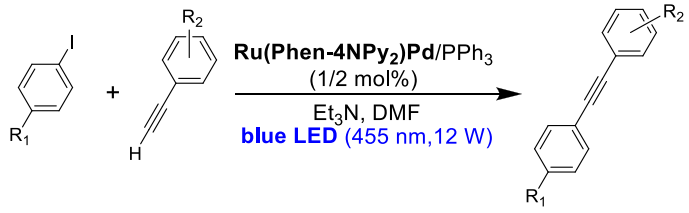

Entry [a]	R_1	R_2	Yield, %	
			22 h [b]	40 h [c]
1	OMe	H	75	95
2	C(O)CH$_3$	H	63	95
3	H	H	81	89
4	H	4-OMe	50	67
5	H	3-COOMe	66	88

[a] Reaction conditions: arylacetylene (0.25 mmol), iodoarene (0.2 mmol), **Ru(Phen-4NPy$_2$)Pd** (1 mol%), Ph$_3$P (2 mol%), Et$_3$N (1 mL), degassed DMF (4 mL), argon atmosphere, Schlenk tube, blue LEDs (12 W), r.t. [b] The yields were determined from NMR ^{1}H analysis of the reaction mixture. [c] Preparative yield.

In order to achieve some degree of understanding of how such a system operates control experiments were performed. The formation of Pd(0) is necessary for the cross-coupling reaction to occur, and it is well known that Pd(0), unlike Pd(II), preferentially forms complexes with phosphines rather than with N-ligands. Moreover the presence of two free sites in the Pd

coordination sphere is required for the reaction to proceed, which excludes the participation of additional *N*-ligands in catalytic cycle. Thus, at the first stage of the reaction, **Ru(L)Pd** complexes can be considered as precatalysts, from which active Pd(0) phosphine complex catalyst $Pd(PPh_3)_2$ is formed. The palladium reduction proceeds through photoinduced electron transfer from the photoexcited Ru(II)-complex to palladium which is supported by absence of the reaction either in in the dark or in the presence of **(NPy$_2$)Pd** complex without the addition of the Ru-complex (Table S19, entries 3, 21). **Ru(Phen-NPy$_2$)Pd** complexes are stable in DMF solution in the dark, but under irradiation they decompose after 12 h (Fig. S52) under the same conditions giving mononuclear Ru(II) complexes due to palladium photoreductionreduction and both DMF and triethylamine taken in excess can act as a reducing agent. Thus, we propose at the initial stage, the formation of the $Pd(PPh_3)_2$ complex occurs, which catalyzes the reaction. **Ru(Phen-NPy$_2$)** complexes showed good photostability in DMF during 24 h of irradiation (Fig. S52). Apparently, 3 hours after the start of the reaction, Pd(0) complex pass into some catalytically inactive form which lead to decrease of the reaction rate in the cases of **Ru(bpy)$_3$/Pd(NPy$_2$)** and **Ru(Phen-5NPy$_2$)Pd** precatalysts. We assume that the formation of a catalytically active complex at the second period occurs with the participation of a **Ru(L)** photocatalyst. Indeed, in the case of the precatalyst **Ru(Phen-3NPy$_2$)Pd**, when the irradiation is turned off after 21 hours, the reaction stops, but when irradiation is resumed, the formation of the product continues. It should be noted that the rate of product formation in the second stage of the reaction is in agreement with data obtained from electrochemical studies, which allow to suggest that catalyst regeneration also may include reduction of palladium. Thus, **Ru(Phen-NPy$_2$)Pd** complexes can be considered as photoswitchable Pd precatalyst.

Our further investigations are aimed at the development of more efficient catalytic systems on the basis of **Phen-NPy** ditopic ligands for Ni/photoredox- and Cu/photoredox-catalyzed reactions.

CONCLUSIONS

A series of novel ditopic ligands – bis(pyridin-2-yl)amino-substituted 1,10-phenanthrolines (**Phen-3NPy$_2$**, **Phen-4NPy$_2$** and **Phen-5NPy$_2$**) differing by the position of an dpa chelating unit in the heterocyclic core were prepared using the copper-catalyzed amination reaction. These ligands were used for the selective two-step synthesis of dinuclear photoactive complexesby stepwise chelation of first Ru(II) to give $[(bpy)_2Ru(\textbf{Phen-NPy}_2)](PF_6)_2$ complexes and then Pd(II) to give $[(bpy)_2Ru(\textbf{Phen-NPy}_2)PdCl_2](PF_6)_2$ complexes in high yields. With the help of NMR and DRX studies we confirmed that the Ru atom is coordinated to 1,10-phenanthroline residue, while the Pd atom is coordinated by dpa moiety. Detailed theoretical and

experimental investigations have been carried out to elucidate the influence of the dpa chelator position on the structure, spectral and electrochemical properties of the synthesized complexes. The complexes **Ru(Phen-4NPy$_2$)Pd** and **Ru(Phen-5NPy$_2$)Pd** were shown to feature the anagostic interaction between palladium and the hydrogen atom of 1,10-phenanthroline moiety in a *peri*-position to dpa moiety. All complexes possess photoluminescence with a maximum at 610–630 nm, quantum yields of Ru complexes exceed that of Ru(bpy)$_3$ and reach 0.15 in the case of **Ru(Phen-4NPy$_2$)**, while for **Ru(Phen-NPy$_2$)Pd** dinuclear complexes it is roughly by order lower and equals 0.018–0.026. All the complexes obtained absorb in the blue region (370–470 nm) and possess extinction coefficient close to [(**L**)Ru(bpy)$_2$] which allow their application as photocatalysts under visible light irradiation. The position of dpa substituent in 1,10-phenanthroline in **Ru(Phen-NPy$_2$)Pd** dinuclear complexes almost does not affect $Ru^{2+/3+}$ redox potential, but influences $Pd^{2+/0}$ potential. For **Ru(Phen-5NPy$_2$)Pd** complex this potential *vs* Ag/AgCl, KCl$_{(sat)}$ was found to be –0.72 V, while for **Ru(Phen-4NPy$_2$)Pd** and **Ru(Phen-3NPy$_2$)Pd** complexes it was –0.57 V. **Ru(Phen-NPy$_2$)Pd** dinuclear complexes have been studied as precatalysts in the visible-light-photoaccelerated Cu-free Sonogashira coupling. The use of **Ru(Phen-4NPy$_2$)Pd** and **Ru(Phen-3NPy$_2$)Pd** complexes provides 3 times higher rate of the model reaction than a mixed catalytic system $Ru(bpy)_3^{2+}$/(RNPy$_2$)PdCl$_2$, while **Ru(Phen-5NPy$_2$)Pd** complex has not shown any advantage. This effect demonstrates a positive effect of combining photocatalyst and metal complex in one structure through the synthesis of ditopic ligands **Phen-4NPy$_2$** и **Phen-3NPy$_2$** whcih make them perspective for hybrid catalysts design for dual metal/photoredox-catalyzed reactions.

EXPERIMENTAL SECTION

Synthesis

General information on materials, methods and synthesis of ligands and complexes is present in the Electronic Supplementary Materials.

X-ray crystallography

Single crystals of the complexes were obtained by slow diffusion of toluene in solutions of complexes in CH_2Cl_2 at room temperature. The measurements for **Ru(Phen-5NPy$_2$)** were made on a Bruker SMART APEX II diffractometer with a CCD area detector (graphite monochromator, Mo-Kα radiation, λ = 0.71073 Å, ω-scanning, $2\theta_{max}$ = 56°). The measurements for other complexes were made on a Bruker D8 Quest diffractometer with a Photon III detector at 100(2) K, MoKα radiation (λ = 0.71073 Å), φ- and ω-scanning. The structures was solved by

direct methods and refined by the full-matrix anisotropic least-squares method on F_2 using SHELXTL and Olex2 program packages.

Structural investigation in solution

All NMR spectra were registered with a Bruker Avance-400 spectrometer in $CDCl_3$ or CD_3CN. 2D NMR spectra of the complexes were recorded on the Agilent 400-MR instrument. Chemical shifts are expressed in parts per million (ppm), referenced on the δ scale by using residual non-deuterated solvent signals as internal standard for ^1H and ^{13}C NMR spectroscopy. The coupling constants are expressed in units of frequency (Hz).

Electrochemical characterization

Voltammetric experiments were performed with Biologic BP-300 potentiostat in a three-electrode electrochemical cell (3 mL volume) at a stationary Pt disk electrode (S = 0.077 cm^2) with a Pt wire counter electrode and Ag/Ag^+ reference electrode (0.01 M $AgNO_3$, 0.1 M Bu_4NBF_4 in MeCN). Fc^+/Fc couple was used as an internal standard in each experiment. The obtained electrochemical data were converted to Ag/AgCl, $KCl_{(s.)}$ reference electrode (the standard potential of Fc^+/Fc couple was taken as 475 mV vs. Ag/AgCl, $KCl_{(s.)}$). Ohmic drop corrections were performed using manual IR compensation procedure implemented in the Biologic software. All solutions were deaerated by passing an argon flow through the solution prior to the CV experiments and above the solution during the measurements. *n*-Bu_4NBF_4 (Aldrich, 99% purity) was used as a supporting electrolyte in all experiments. It was recrystallized from water and dried by heating at 100 °C under high vacuum (0.05 Torr) prior to use. Acetonitrile (AN, Aldrich spectroscopic quality, <0.02% water content) was distilled over P_2O_5. In each case, a freshly distilled portion of the solvent was used.

Photophysical measurements

UV–vis spectra were recorded in solutions using a Hitachi U-2900 UV-vis spectrometer in a quartz cuvette (Hellma, l = 1 cm). Emission spectra were measured in argon saturated acetonitrile solutions using a Horiba Jobin Yvon Fluoromax-2 spectrometer in a quartz cuvette (Hellma, l = 1 cm). Emission quantum yields of all compounds were measured relative to the $Ru(bpy)_3(PF_6)_2$ in argon saturated acetonitrile (Φ_{em} = 0.095) and calculated using a standard procedure.

Photocatalytic Sonogashira coupling

A Schlenk-tube (10 ml) equipped with a magnetic stirrer was charged with aryliodide (0.2 mmol), **Ru(L)Pd**–catalyst (1 mol%), and PPh_3 (2 mol %). The vessel was evacuated and backfilled with dry argon for three times. The vial was sealed with a septum. Then phenylacetylene (0.25 mmol), triethylamine (1 ml) and DMF (4 ml) were added by syringes. The reaction mixture was irradiated at stirring under blue LED irradiation in photoreactor (see ESI, fig. S53). The probe of the reaction mixture (~50-70 μL) was diluted with $CDCl_3$ analyzed by NMR ^1H.

Author contributions

V. A. I., G. S. E., A. A. Y. and A. S. A. performed the synthesis of the ligands and complexes. A. D. S., V. A. I. and A. S. A. performed the photophysical characterization of all complexes. A. D. A. participated in the characterization (NMR and mass spectroscopy) of newly synthesized compounds. V. A. R. performed specific NMR experiments allowing for the signal assignment in the spectra of comlexes. V. E. G and S. E. N. provided single crystal X-ray characterization. A. V. D. and T. V. M. performed the electrochemical characterization of complexes and writing of the original draft of this article section. A. V. C. performed DFT calculations and writing of the original draft of this article section. A. S. A., A. D. A. and I. P. B. were responsible for the project conceptualization, supervision, data analysis, writing and editing of the manuscript and funding acquisition.

Acknowledgements

The authors thank Prof. K. A. Lyssenko for help and useful discussions. This work was supported by the grant of the Ministry for Education and Science of the Russian Federation (agreement of 24.04.2024 no. 075-15-2024-547). The equipment for 2D NMR experiments (Agilent 400-MR spectrometer), X-ray studies (Bruker D8 Quest diffractometer) and microwave-assisted synthesis (Monowave 300 reactor) were purchased by the MSU Development Program.

References

1. T. L. Mako, J. M. Racicot and M. Levine, *Chem. Rev.*, 2019, **119**, 322–477.
2. G. Li, D. Zhu, X. Wang, Z. Su and M. R. Bryce, *Chem. Soc. Rev.*, 2020, **49**, 765–838.
3. S. Tanaka, H. Tsurugi and K. Mashima, *Coord. Chem. Rev.*, 2014, **265**, 38–51.
4. M. Mauro, *Chem. Commun.*, 2021, **57**, 5857–5870.

5. A. Juris, V. Balzani, F. Barigelletti, S. Campagna, P. Belser and A. von Zelewsky, *Coord. Chem. Rev.*, 1988, **84**, 85–277.
6. J. W. Tucker and C. R. J. Stephenson, *J. Org. Chem.*, 2012, **77**, 1617–1622.
7. X. Lang, J. Zhao and X. Chen, *Chem. Soc. Rev.*, 2016, **45**, 3026–3038.
8. M. Shee and N. D. P. Singh, *Catal. Sci. Technol.*, 2021, **11**, 742–767.
9. A. Y. Chan, I. B. Perry, N. B. Bissonnette, B. F. Buksh, G. A. Edwards, L. I. Frye, O. L. Garry, M. N. Lavagnino, B. X. Li, Y. Liang, E. Mao, A. Millet, J. V. Oakley, N. L. Reed, H. A. Sakai, C. P. Seath and D. W. C. MacMillan, *Chem. Rev.*, 2022, **122**, 1485–1542.
10. A. Lipp, S. O. Badir and G. A. Molander, *Angew. Chem. Int. Ed.*, 2021, **60**, 1714-1726.
11. K. Muralirajan and M. Rueping, in *Dual Catalysis in Organic Synthesis 1*, Georg Thieme Verlag KG, Stuttgart, 1st edition edn., 2020, vol. 2019/4.
12. C. Zhu, H. Yue, J. Jia and M. Rueping, *Angew. Chem. Int. Ed.*, 2021, **60**, 17810-17831.
13. Y. Tamaki, K. Watanabe, K. Koike, H. Inoue, T. Morimoto and O. Ishitani, *Faraday Discuss.*, 2012, **155**, 115–127.
14. Y. Tamaki and O. Ishitani, *ACS Catalysis*, 2017, **7**, 3394-3409.
15. L. Zedler, P. Wintergerst, A. K. Mengele, C. Müller, C. Li, B. Dietzek-Ivanšić and S. Rau, *Nat. Commun.*, 2022, **13**, 2538.
16. V. A. Ionova, A. S. Abel, A. D. Averin and I. P. Beletskaya, *Catalysts*, 2023, **13**, 768.
17. G. F. Manbeck and K. J. Brewer, *Coord. Chem. Rev.*, 2013, **257**, 1660–1675.
18. J. Brückmann, C. Müller, I. Friedländer, A. K. Mengele, K. Peneva, B. Dietzek-Ivanšić and S. Rau, *Chem.– Eur. J.*, 2022, **28**, e202201931.
19. M. Lämmle, T. D. Pilz, R. J. Kutta, M. Müßler, A. K. Mengele, H. Görls, F. W. Heinemann and S. Rau, *Dalton Trans.*, 2022, **51**, 15282-15291.
20. Y. Kuramochi, O. Ishitani and H. Ishida, *Coord. Chem. Rev.*, 2018, **373**, 333-356.
21. B. M. Pirzada, A. H. Dar, M. N. Shaikh and A. Qurashi, *ACS Omega*, 2021, **6**, 29291-29324.
22. A. Inagaki, S. Edure, S. Yatsuda and M. Akita, *Chem. Commun.*, 2005, DOI: 10.1039/b508013d, 5468-5470.
23. A. Inagaki, S. Yatsuda, S. Edure, A. Suzuki, T. Takahashi and M. Akita, *Inorg. Chem.*, 2007, **46**, 2432-2445.
24. K. Murata, M. Araki, A. Inagaki and M. Akita, *Dalton Trans.*, 2013, **42**, 6989–7001.
25. S. Kikuchi, K. Saito, M. Akita and A. Inagaki, *Organometallics*, 2018, **37**, 359–366.
26. S. Y. Yao, M. L. Cao and X. L. Zhang, *RSC Advances*, 2020, **10**, 42874–42882.
27. C.-H. Yang, Y.-H. Liu, S.-M. Peng and S.-T. Liu, *Mol. Catal.*, 2022, **522**, 112232.
28. K. Mori, M. Kawashima and H. Yamashita, *Chem. Commun.*, 2014, **50**, 14501–14503.

29. M. Li, X. L. Chia and Y. Zhu, *Chem. Commun.*, 2022, **58**, 4719-4722.
30. L. Bayer, B. S. Birenheide, F. Krämer, S. Lebedkin and F. Breher, *Chem. – Eur. J.*, 2022, **28**, e202201856.
31. W. Iali, P.-H. Lanoe, S. Torelli, D. Jouvenot, F. Loiseau, C. Lebrun, O. Hamelin and S. Ménage, *Angew. Chem. Int. Ed.*, 2015, **54**, 8415-8419.
32. J. Klein, A. Girardon, A. Moreno-Betancourt, F. Loiseau, D. Jouvenot, J. Pécaut, O. Hamelin and S. Torelli, *Eur. J. Inorg. Chem.*, 2023, **26**, e202300397.
33. M. B. Thoke, G.-J. Sun, R. A. Borse, P. Lin and S.-X. Lin, *Org. Chem. Front.*, 2022, **9**, 1797–1807.
34. L. Zedler, C. Müller, P. Wintergerst, A. K. Mengele, S. Rau and B. Dietzek-Ivanšić, *Chem. – Eur. J.*, 2022, **28**, e202200490.
35. T.-J. J. Kinnunen, M. Haukka, M. Nousiainen, A. Patrikka and T. A. Pakkanen, *J. Chem. Soc., Dalton Trans.*, 2001, **2001**, 2649–2654.
36. A. S. Abel, I. S. Zenkov, A. D. Averin, A. V. Cheprakov, A. G. Bessmertnykh-Lemeune, B. S. Orlinson and I. P. Beletskaya, *ChemPlusChem*, 2019, **84**, 498–503.
37. G. V. Morozkov, A. S. Abel, M. A. Filatov, S. E. Nefedov, V. A. Roznyatovsky, A. V. Cheprakov, A. Y. Mitrofanov, I. S. Ziankou, A. D. Averin, I. P. Beletskaya, J. Michalak, C. Bucher, L. Bonneviot and A. Bessmertnykh-Lemeune, *Dalton Trans.*, 2022, **51**, 13612–13630.
38. G. V. Morozkov, A. S. Abel, K. A. Lyssenko, V. A. Roznyatovsky, A. D. Averin, I. P. Beletskaya and A. Bessmertnykh-Lemeune, *Dalton Trans.*, 2024, **53**, 535–551.
39. S. Amthor, P. Keil, D. Nauroozi, D. Perleth and S. Rau, *Eur. J. Inorg. Chem.*, 2021, **2021**, 4790–4798.
40. G. Singh Bindra, M. Schulz, A. Paul, R. Groarke, S. Soman, J. L. Inglis, W. R. Browne, M. G. Pfeffer, S. Rau, B. J. MacLean, M. T. Pryce and J. G. Vos, *Dalton Trans.*, 2012, **41**, 13050–13059.
41. C. Lentz, O. Schott, T. Auvray, G. S. Hanan and B. Elias, *Dalton Trans.*, 2019, **48**, 15567–15576.
42. J. Pang, Y. Tao, S. Freiberg, X.-P. Yang, M. D'Iorio and S. Wang, *J. Mater. Chem.*, 2002, **12**, 206–212.
43. T. Mede, M. Jäger and U. S. Schubert, *Chem. Soc. Rev.*, 2018, **47**, 7577-7627.
44. B.-H. Ye, L.-N. Ji, F. Xue and T. C. W. Mak, *Transition Met. Chem.*, 1999, **24**, 8–12.
45. X. Xiao, J. Sakamoto, M. Tanabe, S. Yamazaki, S. Yamabe and T. Matsumura-Inoue, *J. Electroanal. Chem.*, 2002, **527**, 33–40.
46. W. Huang and T. Ogawa, *Polyhedron*, 2006, **25**, 1379–1385.

47. A. S. Abel, A. Y. Mitrofanov, Y. Rousselin, F. Denat, A. Bessmertnykh-Lemeune, A. D. Averin and I. P. Beletskaya, *ChemPlusChem*, 2016, **81**, 35–39.
48. S. Fakih, W. C. Tung, D. Eierhoff, C. Mock and B. Krebs, *Z. Anorg. Allg. Chem.*, 2005, **631**, 1397-1402.
49. J. E. Aguado, O. Crespo, M. C. Gimeno, P. G. Jones, A. Laguna and Y. Nieto, *Eur. J. Inorg. Chem.*, 2008, **2008**, 3031-3039.
50. M. Brookhart, M. L. H. Green and G. Parkin, *Proc. Natl. Acad. Sci. U.S.A.*, 2007, **104**, 6908–6914.
51. V. Balzani, A. Juris, M. Venturi, S. Campagna and S. Serroni, *Chem. Rev.*, 1996, **96**, 759–834.
52. H. Suzuki, T. Kanbara and T. Yamamoto, *Inorg. Chim. Acta*, 2004, **357**, 4335–4340.
53. A. S. Abel, A. D. Averin, A. V. Cheprakov, I. P. Beletskaya, M. Meyer and A. Bessmertnykh-Lemeune, *Chemosensors*, 2022, **10**, 79.
54. A. Ghosh, B. Ganguly and A. Das, *Inorg. Chem.*, 2007, **46**, 9912–9918.
55. A. M. Brouwer, 2011, **83**, 2213–2228.
56. H. Nitadori, T. Takahashi, A. Inagaki and M. Akita, *Inorg. Chem.*, 2012, **51**, 51-62.
57. A. A. Granovsky, *Firefly version 8,* www *http://classic.chem.msu.su/gran/firefly/index.html*.
58. M. W. Schmidt, K. K. Baldridge, J. A. Boatz, S. T. Elbert, M. S. Gordon, J. H. Jensen, S. Koseki, N. Matsunaga, K. A. Nguyen, S. Su, T. L. Windus, M. Dupuis and J. A. Montgomery Jr, *J. Comput. Chem.*, 1993, **14**, 1347–1363.
59. C. L. Barros, P. J. P. de Oliveira, F. E. Jorge, A. Canal Neto and M. Campos, *Mol. Phys.*, 2010, **108**, 1965–1972.
60. D. F. Zigler, Z. A. Morseth, L. Wang, D. L. Ashford, M. K. Brennaman, E. M. Grumstrup, E. C. Brigham, M. K. Gish, R. J. Dillon, L. Alibabaei, G. J. Meyer, T. J. Meyer and J. M. Papanikolas, *J. Am. Chem. Soc.*, 2016, **138**, 4426–4438.
61. M. Osawa, H. Nagai and M. Akita, *Dalton Trans.*, 2007, DOI: 10.1039/B618007H, 827–829.
62. K. C. Dissanayake, P. O. Ebukuyo, Y. J. Dhahir, K. Wheeler and H. He, *Chem. Commun.*, 2019, **55**, 4973–4976.